ISSN 1070-3284, Russian Journal of Coordination Chemistry, 2020, Vol. 46, No. 11, pp. 779–785. © Pleiades Publishing, Ltd., 2020.
Russian Text © The Author(s), 2020, published in Koordinatsionnaya Khimiya, 2020, Vol. 46, No. 11, pp. 706–712.

The authors congratulate Academician I.L. Eremenko on his 70th jubilee

Structure and Noncovalent Interactions of Molybdenum Disulfide Monolayers in the Layered Organo-Inorganic Compound with Tetramethylguanidine

I. E. Ushakov[a], A. S. Goloveshkin[a], N. D. Lenenko[a], R. U. Takazova[a], M. G. Ezernitskaya[a], A. A. Korlyukov[a], V. I. Zaikovskii[b, c], and A. S. Golub'[a, *]

[a] *Nesmeyanov Institute of Organoelement Compounds, Russian Academy of Sciences, Moscow, 119991 Russia*
[b] *Boreskov Institute of Catalysis, Siberian Branch, Russian Academy of Sciences, Novosibirsk, Russia*
[c] *Novosibirsk State University, Novosibirsk, Russia*
**e-mail: golub@ineos.ac.ru*

Received March 14, 2020; revised April 1, 2020; accepted April 8, 2020

Abstract—A layered compound with regularly alternating monolayers of MoS_2 and *N*,*N*,*N*',*N*'-tetramethylguanidine (TMG) is synthesized by the reaction of monolayer dispersions of molybdenum disulfide containing anionic particles $(MoS_2)^{x-}$ with protonated TMG molecules. It is found by a combination of methods (X-ray diffraction analysis adapted for turbostrate-disordered systems, high-resolution transmission electron microscopy, FT-IR spectroscopy, and quantum-chemical calculations by the density functional theory) that the structure of MoS_2 layers with octahedrally coordinated molybdenum atoms forming chains of Mo–Mo bonds is stabilized in the compound. Noncovalent binding interactions occur between the MoS_2 monolayers and TMG molecules including CH...S, NH...S, and N...S contacts with the predominant contribution of contacts of the first type to the binding energy (CIF file CCDC no. 1990439).

Keywords: molybdenum disulfide, organo-inorganic compounds, structure, noncovalent interactions, hydrogen bonds

DOI: 10.1134/S1070328420090067

INTRODUCTION

Molybdenum disulfide is one of the most demanded layered materials, which exists in the nature and produced by the industry. Owing to unique structural and physicochemical properties, the material is applied in petrochemical catalysts [1] and lubricants [2] and is used in promising developments of thin-layer electronic devices [3], electrocatalysts [4], energy stores [5], biosensors [6], and bioactive drugs [7]. The insertion of organic molecules into the interlayered space of MoS_2 crystals is an efficient tool for the modification of structural properties of this material, including a change in the coordination mode of molybdenum atoms with sulfur in the layers (from trigonal prism to octahedron) and can be used for affecting the conducting and catalytic properties of the material [4, 5].

The elucidation of structure forming interactions in layered organo-inorganic compounds of molybdenum disulfide is an important task for their target design. Since the character of superposition of heterolayers in particles of the MoS_2 compounds is turbostrate, a complex approach including the simulation of diffraction patterns of turbostrate-disordered systems according to Ufer [8] and quantum-chemical optimization of structural models [9, 10] is needed to obtain necessary structural information. The structures of the layered MoS_2 compounds with several types of nitrogen-containing organic molecules were determined in the recent years using this approach. It was found that hydrogen bonds between the sulfur atoms of the MoS_2 layers and organic guests played an important role in the stabilization of the spatial structures of these compounds including the octahedral coordination in the MoS_6 polyhedron necessary for a series of application. For example, in the case of intercalated tetraalkylammonium cations, weak CH...S interactions, being the only specific interactions with sulfide layers accessible for these compounds, determine the positions of the molecules relative to the nanorelief of the sulfide layers forcing the cations to arrange in nanohollows on the layer surface [9]. It was

Table 1. Structural parameters of the layered compound $(TMG)_{0.13}MoS_2$

Parameter*	Value
Space group	*P*1
a, Å	5.685(9)
b, Å	3.208(5)
c, Å	10.19(1)
Shortest distances Mo–Mo, Å	2.806(10); 3.208(5); 3.751(11)
Angle MoMoMo in zigzags, deg	69.7(3)
S–S $\Delta z1$, $\Delta z2$, Å	3.440(12), 2.201(12)
Height drop of nanorelief of layers, Å	0.620(12)
Shift of MoS_2 layers, Å	
along axis *a*	3.411(6)
along axis *b*	2.438(6)
*R*wp, %	3.267

* $\alpha = \beta = \gamma = 90°$.

found that the same interactions were responsible for the arrangement of alkylenediamine molecules in nanohollows, whereas the slope of these molecules relative to the sulfide layers is caused by the formation of strong hydrogen bonds NH...S with both adjacent sulfide layers [11].

The atomic structures and binding contacts for the layered MoS_2 compounds containing only amino(ammonium) groups $NH_2(NH_3^+)$ have previously been determined [11]. Therefore, the study of the interactions of MoS_2 with other NH-donors and the evaluation of the influence of their geometry on the architecture of the compounds are of doubtless interest.

In this work, we synthesized the new layered compound $(TMG)_{0.13}MoS_2$ (**I**) containing protonated molecules of *N*,*N*,*N*',*N*'-tetramethylguanidine (TMG), which willingly form strong hydrogen bonds with various anions [12, 13], determined its structure, and examined the energy characteristics of the binding contacts.

EXPERIMENTAL

Synthesis of $(TMG)_{0.13}MoS_2$ (I) was carried out by the reaction of a monolayer dispersion of $LiMoS_2$ with protonated TMG molecules similarly to the related compounds MoS_2 described earlier [10, 11]. For this purpose, compound $LiMoS_2$ was first synthesized by the treatment of natural powdered MoS_2 (DM-1 trade mark, Skopinskii Plant, Skopin, Russia) with an excess 1.6 M solution of *n*-butyllithium in hexane (Aldrich) at 20°C for one week followed by washing with hexane and drying in vacuo. Then $LiMoS_2$ (0.1000 g, 5.99 mmol) was dispersed in a solution (100 mL) containing TMG (Aldrich) (0.1721 g, 15.0 mmol) in water acidified with HCl with argon bubbling and ultrasonic treatment. The reaction mixture was magnetically stirred for 2 h, and the formed precipitate of the compound was filtered off, washed three times with water, and dried in vacuo. The yield was 0.9960 g (95%). The composition of the compound was determined by the elemental analysis data.

For $(C_5H_{14}N_3)_{0.13}S_2Mo$

Anal. calcd., %	C, 4.46	H, 1.04	N, 3.12	Mo, 54.83
Found, %	C, 4.43	H, 1.25	N, 3.02	Mo, 54.70

High-resolution transmission electron microscopy (HRTEM) images were obtained on a JEM-2200FS instrument (JEOL Ltd.) with a limiting resolution for lines of 0.1 nm and an accelerating voltage of 200 kV. Samples for the study were placed on perforated carbon supports fixed on standard copper lattices and then were placed in a chamber of the electron microscope. The Fourier filtration (FFT) and analysis of HRTEM images with the determination of interplanar distances were performed using the Digital Micrograph 3.6.5 program (Gatan Inc.).

Attenuated internal reflection (ATR) FT-IR spectra were recorded on a Vertex 70v FT-IR spectrometer (Bruker, Germany) using a PIKE accessory for ATR (USA) with the diamond working unit. The spectra were recorded in vacuo in a spectral range of 4000–400 cm^{-1} with a resolution of 4 cm^{-1}. Necessary corrections were applied using the Omnic 8 spectral program (Nicolet, United States).

The X-ray diffraction (XRD) study of the compound was conducted on a Bruker D8 Advance Vario diffractometer (Bruker AXS) equipped with an X-ray tube with a copper anode, a germanium monochromator, and a Lynx-Eye position-sensitive detector in the X-ray transmission geometry. The recording step was 0.01° 2θ in the range 6°–90° 2θ. The XRD images were simulated using the TOPAS 5 program (Bruker AXS). Selected structural characteristics of the layered compound are presented in Table 1.

The coordinates of atoms and other parameters of the structure were deposited with the Cambridge Crystallographic Data Centre (CIF file CCDC no. 1990439; https://www.ccdc.cam.ac.uk/structures).

The quantum-chemical calculation was performed using the VASP program (version 5.3) [14, 15]. The atomic coordinates were optimized using the PBE exchange-correlation functional in the plane wave basis set (maximum kinetic energy 545 eV) and the Grimme D3 dispersion correction [16]. The "rigid" PAW (projected augmented wave) potentials [17] were used for the description of core electrons (the least size of the area described by the pseudowave function). The calculated electron density function was obtained using the maximum kinetic energy equal to 1360 eV.

The topological analysis was performed using the AIM program implemented in the ABINIT program package [18].

RESULTS AND DISCUSSION

It is known that the assembling of compounds in an aqueous monolayer dispersion of MoS_2 containing negatively charged monolayer particles $(MoS_2)^{x-}$ leads to the formation of layered structures with the anionic monolayers alternating with the monolayers of organic cations (A^+) according to Eq. (1) [10]. When highly basic TMG (pK_a 13) is involved in the assembling, only the protonated form of TMG molecules ($TMGH^+$), which predominates in the solution in a wide pH range, can act as cations.

$$\left[Li^+ + (MoS_2)^{x-} + (1-x)OH^-\right]_{aq} + xA^+ \rightarrow \left(A^+\right)_x (MoS_2)^{x-}. \quad (1)$$

The incorporation of TMG molecules in the organo-inorganic compound is confirmed by both the elemental analysis data and FTIR-ATR spectra (Fig. 1). The spectrum of compound **I** distinctly shows the main bands of the initial TMG, although the ratio of intensities between the spectra differs substantially. The differences can be related to a distortion of the spatial structure of the TMG molecule upon the incorporation into the compound, interaction with the surface of the sulfide layers, and other physical factors. Note that the bands at 3323 and 3300 cm^{-1} caused by vibrations of the free (or weakly bound) NH (TMG) or NH_2^+ group (**I**), respectively, appear in the ν(NH) vibration range of the spectra of TGM and compound **I**. In both cases, there is no broad absorption in a range of 3400–2700 cm^{-1} characteristic of the corresponding group involved in the strong hydrogen bond [19].

This shows, in particular, that the $TMGH^+$ cations in the compound MoS_2 are not associated with neither neutral TMG molecules, nor water molecules.

The HRTEM study of compound **I** made it possible to establish that compound **I** precipitated from dispersions as platy particles. The typical lateral projection of the particle is shown in Fig. 2. The particles are formed by packages of regularly arranged MoS_2 layers with broadened (compared to the phase of pure MoS_2) interlayer gaps, which is caused by the intercalation of guest molecules, as in the case of the earlier MoS_2 compounds with organic molecules [10, 11, 20]. As can be seen from the HRTEM images, the periodicity in the arrangement of the layers determined from the Fourier samples of the fragments of the structure and by the intensity profiles in the direction perpendicular to the layers is 9.6–1.1 Å. These layers are well consistent with the powder X-ray diffraction data, which showed an increase in the interlayer periodicity in the hybrid structure from 6.15 Å (initial MoS_2, space group $P6_3/mmc$, the diffraction pattern completely corresponds to JCPDS-77-1716) to 10.2 Å (Fig. 3).

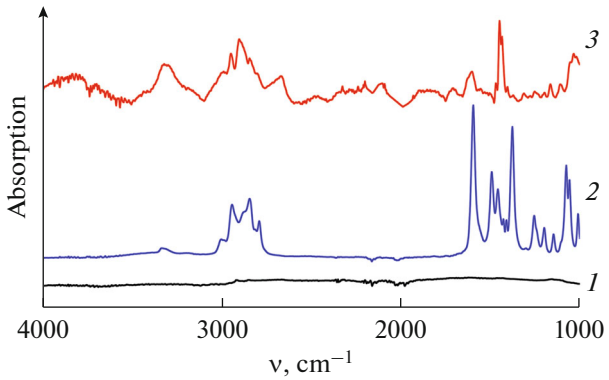

Fig. 1. FTIR-ATR spectra of (*1*) MoS_2, (*2*) TMG, and (*3*) $(TMG)_{0.13}MoS_2$.

As can be seen from Fig. 3, the XRD pattern of the compound exhibits basal 00*l* reflections, whose positions are due to the interlayer distance between the MoS_2 layers, and the *hk*0 zone (in the range $2\theta > 30°$) with a set of asymmetric broadened reflections typical of the 2D-ordered structures with the turbostrate superposition of the layers, for example, layered clays [8]. The diffraction profile was simulated as described previously [9, 10, 20] using Ufer's supercell [8], whose periodicity along the *c* axis (perpendicularly to the MoS_2 layers) is amplified by 20 times compared to the interlayer distance in the compound. The cell (space group $P1$) contained two MoS_2 layers with the associated organic molecules, which allowed relationships in the layer superposition to be revealed [10]. The Rietveld refinement of the model made it possible to determine the structure of the MoS_2 layers, their systematic shifts relative to one another, and arrangement of the organic molecules (Figs. 4, 5). The main structural characteristics of the compound are presented in Table 1.

The data obtained indicate that the geometry of the MoS_2 monolayer in compound **I** corresponds to the modification 1T, which was observed in the earlier studied MoS_2-based organic compounds [9, 10, 20]. The modification differs from the usual modification 2H characteristic of natural molybdenite by both the octahedral coordination of molybdenum with sulfur (instead of trigonal prismatic) and nonequivalent Mo–Mo distances caused by the formation of chains of the molybdenum atoms in the plane of the sulfide layer, as well as by the corrugated sublattice of the sulfur atoms (Figs. 4, 5). The corrugation appears due to the formation of nanosized projections and hollows propagated over the surface of the MoS_2 monolayer along the *b* axis. In the studied compound, the drop of the relief heights is 0.62 Å, which exceeds by

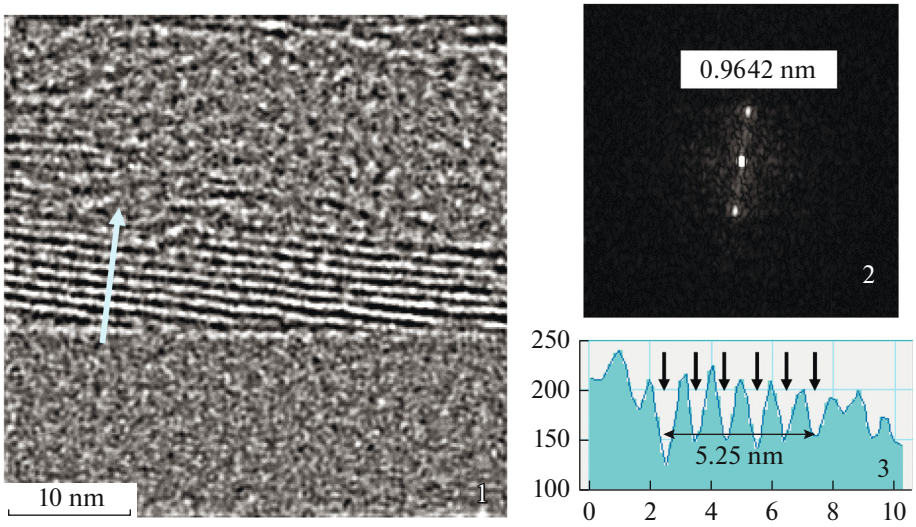

Fig. 2. (1) HRTEM image of the fragment of the structure of compound **I**, (2) its FFT image, and (3) intensity profile along the line.

~1.5 times the typical value of this parameter for the earlier studied MoS_2 compounds with organic guests [10, 11, 20]. In addition, we can mention the high systematic shifts of the MoS_2 monolayers relative to each other appeared upon the assembling of particles of layered compound **I** compared to the previously studied compounds. The shift of the layers along the *a* axis of Ufer's cell is ~3.41 Å (or 2.27 Å with allowance for parameter *a*), whereas the absolute values of the shifts did not exceed 1 Å for other compounds. Both these facts indicate that the geometry of the MoS_2 monolayers is tuned to the geometry of the molecules coordinated with them to provide the most efficient binding.

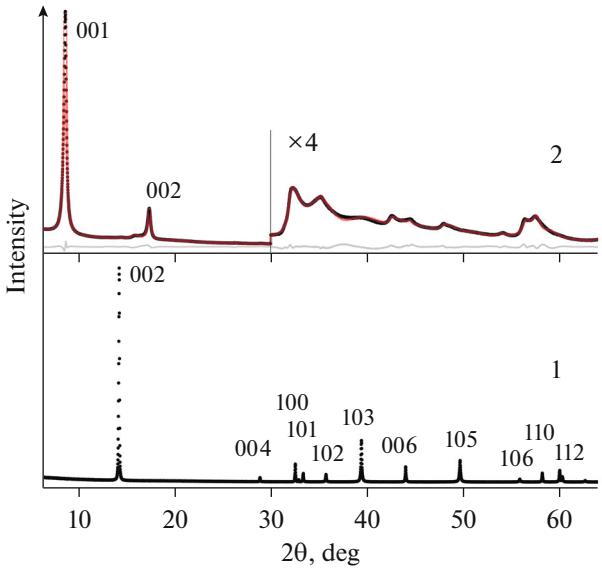

Fig. 3. Experimental XRD patterns of (1) initial MoS_2 and (2) $(TMG)_{0.13}MoS_2$ (black points): calculated XRD pattern (red line) and differential curve (gray line) for the layered compound.

The plane of the guanidine fragment of the TMG molecules is arranged at a slight slope toward the MoS_2 layers (19°), and the NH_2 group is directed toward the sulfur atom located in the nanohollow on the layer surface. The methyl substituents also tend to occupy positions above the hollows of the sulfide layer to which this substituent is closest.

To reveal the binding interactions in compound **I**, we used the obtained structural data to construct the model of hypothetical ordering of the crystal without turbostrate character in the layer superposition. For this purpose, by analogy to the earlier studied compounds of this type [10, 11, 20], the partially populated positions were uniformly occupied by the cations according to their content avoiding short contacts between the molecules (Fig. 5). The composition of this periodical structure, $(TMG)_{1/6}MoS_2$, is close to the experimentally found stoichiometry of compound **I**. The model was described by the triclinic cell, whose parameters (a = 6.523, b = 9.6297, c = 10.467 Å, α = 94.20°, β = 98.77°, γ = 119.78°) were related to the parameters of Ufer's cell used for structure refinement by the following equations: $\bar{a} = \bar{a}_{ref} - \bar{b}_{ref}$, $\bar{b} = 3\bar{b}_{ref}$, and $\bar{c} = \bar{c}_{ref}/N + \bar{S}$, where indices *ref* designate the parameters of the refined cell, and $\bar{S}$ is the layer shift vector.

The DFT (PBE-D3/PW) quantum-chemical calculations were performed to optimize the geometry of compound **I** and to calculate the function of the calculated electron density distribution ($\rho(r)$). An analysis of the obtained distribution according to Bader's theory "Atoms in Molecules" revealed the critical points (CP) (3, –1) on the bonding routes in the compound.

The properties of the CP of the bonds inside the MoS_2 layers and between them and TMG molecules are presented in Table 2. It is important that inside the MoS_2 layer the calculation shows the appearance of the CP corresponding to the formation of Mo–Mo bonds, which are absent in the initial MoS_2 with the trigonal prismatic coordination of Mo–S [21]. It is also noteworthy that the lengths and energy characteristics of the CP of the Mo–S bonds are nonequivalent, which is due to the formation of the relief surface of the S–Mo–S layer with projections and hollows.

The energies of noncovalent interactions involving the TMG cations (E_{cont}) were estimated using the Espinosa–Molins–Lecomte relationship between the potential energy density of the CP and bond energy [22, 23]. The values obtained for E_{cont} are presented in Table 3. According to the calculations, the total energy of the cation–MoS_2 interaction is 20.7 kcal/mol, and fairly weak CH...S interactions characterized by an average contact energy of ~1 kcal/mol make the predominant contribution (~73%) to the total energy. It should be mentioned that a significant contribution of the aliphatic fragments to the stabilization of the structures of compounds MoS_2 was also observed for other guest molecules involved in several competitive types of binding with the MoS_2 layers. The contribution of the CH...S interactions to the stabilization of the structures of the MoS_2 compounds with alkylenediamine molecules reached 20–60% depending on the geometry of diamine, and the highest contribution was provided by the branched structure of the tetramethylethylenediamine type [11]. Evidently, this binding is favored by the incorporation of the alkyl substituents into hollows of the nanorelief, which provides an increase in the number of CH...S contacts. This is an important factor affecting the packing of the organic molecules between the molybdenum disulfide layers.

According to the calculated data, the hydrogen bonds of the NH_2 group make a less significant energy contribution to the stabilization of the compound (~16%). The strongest bond with an energy of 2.51 kcal/mol is characterized by a distance H–S of 2.540 Å and an angle NHS of 153°. A still lower contribution (~11%) provides the participation in *p*-electron binding of the conjugated system of bonds of the cationic guanidine fragment, which is likely due to the shielding of the nitrogen atoms by the methyl substituents preventing the formation of short N...S contacts.

Thus, the interaction of the negatively charged monolayer particles $(MoS_2)^{x-}$ with cationic protonated TMG molecules afforded heterolayer compound **I** with regularly alternating organic (TMG) and inorganic (MoS_2) layers. The structures of the MoS_2 and guest layers were determined using HRTEM, FT-IR spectroscopy, simulation of the powder diffraction patterns of the turbostrate-disordered compounds, and quantum-chemical calculations. It is found that the structure with the octahedrally coordinated molybdenum atoms forming chains of the Mo–Mo bonds, which differs from the most stable modification of MoS_2 with the trigonal prismatic coordination, is stabilized in these layers due to the incorporation of TMG between the MoS_2 layers. This is consistent with the results of studying other MoS_2-based organic compounds. The binding interactions inside the sulfide layers and between them and TMG molecules were revealed by the calculated electron density distribution and were analyzed according to Bader's theory. The

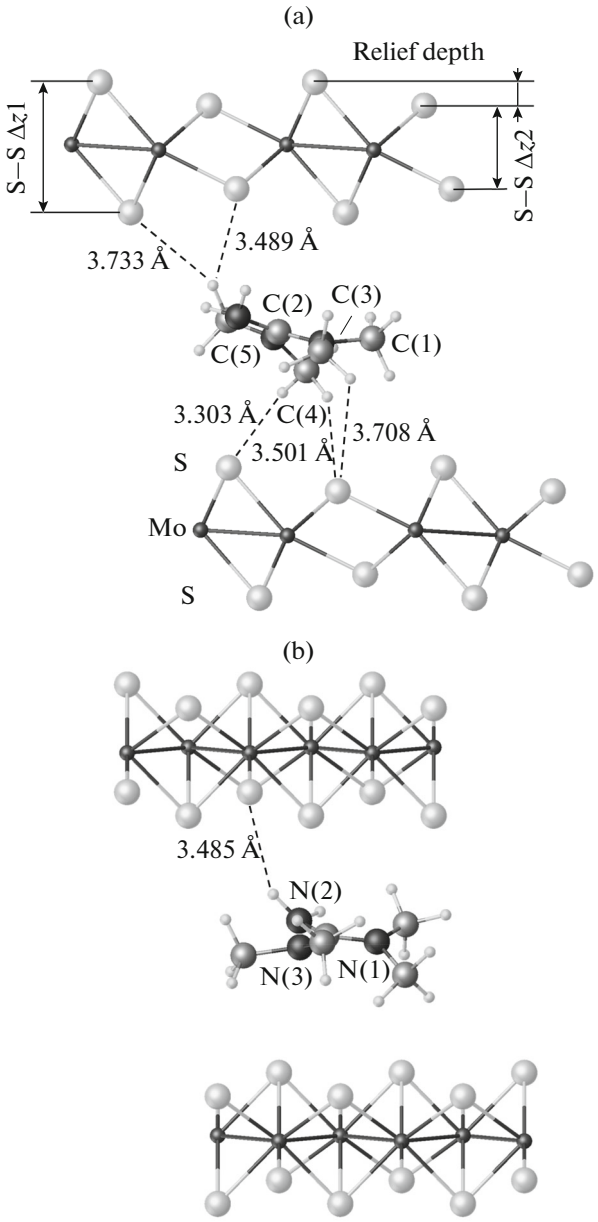

Fig. 4. Structure of compound **I** in the projection along the (a) *b* and (b) *a* axes. Short contacts CH...S and NH...S with the distance and interaction energy (kcal/mol) are shown.

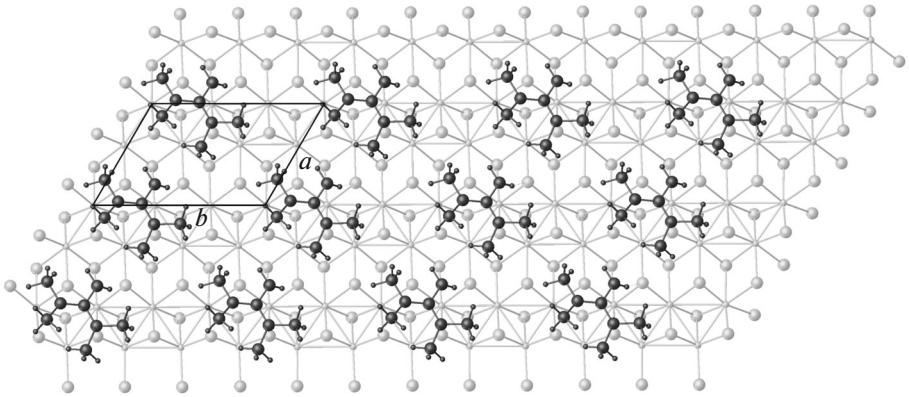

Fig. 5. Arrangement of the TMG molecules on the MoS_2 layer in the optimized structure.

Table 2. Characteristics of the bonding critical points (3, –1) in $(TMG)_{1/6}MoS_2$*

Interaction	Number of interactions	Distance between atoms, Å	$\rho(r)$	$\nabla^2\rho(r)$	$G^e(r)$	$V^e(r)$	$H^e(r)$
Mo...Mo	6	2.843	0.064711	0.105991	0.047635	–0.06877	–0.02114
Mo...S	18	2.421	0.095457	0.179022	0.087113	–0.12947	–0.04236
Mo...S	18	2.485	0.083042	0.138066	0.068426	–0.10233	–0.03391
NH...S	2	3.485–3.843	0.009366	0.024927	0.005555	–0.00488	0.000677
N...S	3	3.451–3.843	0.005796	0.016889	0.003391	–0.00256	0.000831
CH...S	16	3.489–4.120	0.006541	0.018876	0.003875	–0.00303	0.000844

* $\rho(r)$ is the electron density, $\nabla^2\rho(r)$ is the electron density Laplacian, $G^e(r)$ is the kinetic electron energy density, $V^e(r)$ is the potential electron energy density, and $H^e(r)$ is the local electron energy density.

noncovalent interactions TMG–MoS_2 include the CH...S, NH...S, and N...S contacts with the predominant contribution of the first type contacts to the binding energy. The data obtained can be expected to be useful for the targeted design of the organo-inorganic compounds based on molybdenum disulfide.

ACKNOWLEDGMENTS

The structural studies were supported by the Ministry of Science and Higher Education of the Russian Federation using the scientific equipment of the Center of Investigation of Structure of Molecules of the Nesmeyanov Institute of Organoelement Compounds (Russian Academy of Sciences).

Table 3. Energy of binding noncovalent interactions (E_{cont}) of the $TMGH^+$ cations (kcal/mol per mole of cation)

Type of bond	Number of contacts	E_{cont}
CH...S	16	15.2
NH...S	2	3.1
N...S	2	2.4
Caton...MoS_2	20	20.7

FUNDING

This work was supported by the Russian Science Foundation, project no. 20-13-00241.

CONFLICT OF INTEREST

The authors declare that they have no conflicts of interest.

REFERENCES

1. Startsev, A.N. and Zakharov, I.I., *Russ. Chem. Rev.*, 2003, vol. 72, p. 517.
2. Tannous, J., Dassenoy, F., Lahouij, I., et al., *Tribol. Lett.*, 2011, vol. 41, p. 55.
3. Jariwala, D., Howell, S.L., Chen, K.-S., et al., *Nano Lett.*, 2016, vol. 16, p. 497.
4. Benck, J.D., Hellstern, T.R., Kibsgaard, J., et al., *ACS Catal.*, 2014, vol. 4, p. 3957.
5. Yoo, H.D., Li, Y., Liang, Y., et al., *ChemNanoMat*, 2016, vol. 2, p. 688.
6. Kalantar-Zadeh, K. and Ou, J.Z., *ACS Sensors*, 2016, vol. 1, p. 5.
7. Yin, F., Anderson, T., Panwar, N., et al., *Nanotheranostics*, 2018, vol. 2, p. 371.

8. Ufer, K., Roth, G., Kleeberg, R., et al., *Z. Kristallogr.*, 2004, vol. 219, p. 519.
9. Goloveshkin, A.S., Lenenko, N.D., Zaikovskii, V.I., et al., *RSC Adv.*, 2015, vol. 5, p. 19206.
10. Goloveshkin, A.S., Lenenko, N.D., Zaikovskii, V.I., et al., *Langmuir*, 2015, vol. 31, p. 8953.
11. Ushakov, I.E., Goloveshkin, A.S., Lenenko, N.D., et al., *Cryst. Growth Des.*, 2018, vol. 18, p. 5116.
12. Dong, K., Zhang, S., and Wang, J., *Chem. Commun.*, 2016, vol. 52, p. 6744.
13. Berg, R.W., Riisager, A., Buu, O.N.V., et al., *J. Phys. Chem. A*, 2010, vol. 114, p. 13175.
14. Kresse, G. and Furthmüller, J., *Comput. Mater. Sci.*, 1996, vol. 6, p. 15.
15. Kresse, G. and Furthmüller, J., *Phys. Rev. B: Condens. Matter Mater. Phys.,* 1996, vol. 54, p. 11169.
16. Grimme, S., *J. Comput. Chem.*, 2006, vol. 27, p. 1787.
17. Kresse, G. and Joubert, D., *Phys. Rev. B: Condens. Matter Mater. Phys.,* 1999, vol. 59, p. 1758.
18. Gonze, X., Beuken, J.-M., Caracas, R., et al., *Comput. Mater. Sci.*, 2002, vol. 25, p. 478.
19. Galezowski, W., Jarczewski, A., Stanczyk, M., et al., *J. Chem. Soc., Faraday Trans.*, 1997, vol. 93, p. 2515.
20. Goloveshkin, A.S., Bushmarinov, I.S., Korlyukov, A.A., et al., *Russ. J. Inorg. Chem.*, 2017, vol. 62, p. 729. https://doi.org/10.1134/S0036023617060080
21. Naumov, N.G., Korlyukov, A.A., Piryazev, D.A., et al., *Russ. Chem. Bull.*, 2013, vol. 62, p. 1852.
22. Espinosa, E., Molins, E., and Lecomte, C., *Chem. Phys. Lett.*, 1998, vol. 285, nos. 3–4, p. 170.
23. Espinosa, E., Lecomte, C., and Molins, E., *Chem. Phys. Lett.*, 1999, vol. 300, p. 745.

Translated by E. Yablonskaya